Ceramics-Silikáty 65 (1), 1-8 (2021)
www.ceramics-silikaty.cz doi: 10.13168/cs.2020.0036

PREPARATION AND CHARACTERIZATION OF TiO_2–Ta_2O_5–$CaCO_3$ VARISTOR CERAMICS BY HOT ISOSTATIC PRESSING (HIP) AND POST-ANNEALING

KUNYONG KANG*, **, ***, GANG ZHU*, **, ***, XIJUAN CHAI*, **, ***,
SHUDUAN DENG*, **, ***, #KAIMENG XU*, **, ***

*Yunnan Key Laboratory of Wood Adhesive and Glued Product, Southwest Forestry University, Kunming 650224, PR China
**Functional and Wood-based Ceramics Laboratory, Southwest Forestry University, Kunming 650224, PR China
***School of Materials Science and Engineering, Southwest Forestry University, Kunming 650224, PR China

#E-mail: xukm007@163.com

Submitted July 1, 2020; accepted september 21, 2020

Keywords: Titanium oxide (TiO_2), Varistor ceramics, Nonlinear coefficient, Breakdown voltage, Hot Isostatic Pressing (HIP), Post-Annealing

TiO_2–Ta_2O_5–$CaCO_3$ varistor ceramics were prepared by hot isostatic pressing (HIP) and annealed in oxygen and nitrogen, respectively. The nonlinear coefficient α, the breakdown voltage EB and the leakage current JL of samples were tested using a varistor dc parameter meter. The average barrier height Φ_B of the unannealed samples and the samples annealed in oxygen and nitrogen was calculated. The microstructure of samples was analyzed by STEM-EDS, XRD and SEM. TiO_2–Ta_2O_5–$CaCO_3$ varistor ceramics with uniform microstructure, fine grains and low porosity was obtained by HIP. By annealing, α increases, while E_B and J_L decrease. When annealing is performed in oxygen, the oxygen enrichment at the grain boundaries is also helpful to increase α and reduce JL. TiO_2–Ta_2O_5–$CaCO_3$ varistor ceramics with Ta_2O_5 and $CaCO_3$ contents of 0.20 mol. % sintered at 1200 °C and annealed at 700 °C for 3 h in oxygen possesses best varistor performance with α = 11.2, E_B = 22.6 V·mm^{-1} and J_L = 8.7 μA·cm^{-2}.

INTRODUCTION

Because of nonlinear electrical behavior and sensitivity to instantaneous voltage fluctuations, varistor ceramics are widely used in circuits such as overvoltage protection, high voltage stability and high energy surge absorption [1-3]. The nonlinear behavior of a varistor is closely associated with the grain boundary barrier structure of polycrystalline ceramics [4]. Compared with other varistor ceramics, TiO_2 varistor ceramics have the advantages of low breakdown voltage and good dielectric performance, which can be used as a varistor-capacitor multifunctional material with simple preparation process and low cost [5-8]. Therefore they have a good application perspective [9-13]. But its nonlinear coefficient α (i.e. the ratio of static resistance to dynamic resistance at a point on an I-V curve) is generally quite low, which limits its practical application. Since TiO_2 ceramics was found to exhibit varistor characteristics in the Bell Labs in 1982 [4], researchers tried to improve its α value. Many works studied the effects of donor single doping, acceptor single doping and co-doping on the varistor properties [14-17].

Annealing is a heat treatment process in which samples are heated to a suitable temperature, kept for a period of time and then slowly cooled to obtain an equilibrated microstructure with required properties. Annealing can stabilize size, adjust microstructure, eliminate defects and residual stress. Zheng et al. studied the effect of annealing on GaN-based semiconductor capacitors prepared by atomic deposition. The results suggest that the capacitance increases gradually as the annealing temperature increases from 300 to 500 °C [18]. Priyadarshini et al. studied the influence of the annealing environment on a SnO_2 thin film transistor deposited by the spin coating technique. The films are annealed at 500 °C for 1 h in different annealing ambient conditions with varying N_2:O_2 ratio. The results reveal that with the increase in nitrogen concentration the amount of defects in the films increases, but the device performance improves [19]. Hosokawa et al. studied the effect of annealing on the properties of Nd–Fe–Ti–B magnets. The results show that the magnetic properties can be improved by annealing for a short time at a temperature close to the crystallization temperature, while further annealing at a high temperature for a long time will lead to the deterioration of the magnetic properties [20]. Ramanjaneyulu et al. studied the reversible p-type properties of (P, N) co-doped ZnO films by pulse laser deposition. As the film grows, it changes from p-type to *n*-type within 120 days. Unannealed n-type films contain the donor impurities hydrogen and carbon, which are transformed into p-type semiconductors after annealing at 800 °C [21]. Li et al. studied annealing effects on the

structural and optical properties of TiO_2 films. The results show that the band gap of TiO_2 thin films decreases when the annealing temperature increases [22]. Mohsen et al. studied $CaCu_3Ti_4O_{12}$ (CCTO) thin films deposited by radio frequency magnetron sputtering and subsequently annealed at 300, 400, 500 or 600 °C. XRD analysis shows that the amorphous CCTO thin film transforms to a more crystalline structure as the annealing temperature increases to 600 °C [23].

In this work, in order to improve the nonlinear coefficient α of TiO_2 varistor ceramics, reduce the breakdown voltage E_B and the leakage current J_L, TiO_2–Ta_2O_5––$CaCO_3$ varistor ceramics were prepared by hot isostatic pressing (HIP) sintering and annealed in different atmospheres. After annealing the microstructure and varistor properties were investigated.

EXPERIMENTAL

The mixture was ground in a planetary ball mill to obtain the reactants. The purity of each reagent is as follows: TiO_2 (powder, 99.9 %), Ta_2O_5 (powder, 99.9 %), $CaCO_3$ (powder, 99.9 %). All reagents were obtained from Guanghua Sci-tech (China). Table 1 shows the initial doping content of the samples. According to the ratio of raw materials in Table 1, the mixture was ground for 10h with a mass ratio of 1:2:4 of powder to water blended with alcohol (water:alcohol = 3:1) to balls. After homogenization, each blend was dried at 90 °C for 10 h and de-agglomerated in a 400 mesh sieve. The obtained powder was isostatically pressed at 160 MPa into tablets (10 mm in diameter and 1mm thick). The tablets were degummed at 500 °C for 1 h in a box-type resistance furnace and cooled to room temperature. The degummed tablets were sintered for 2 h at 1100, 1150, 1200, and 1250 °C, respectively, in a hot isostatic pressing (HIP) furnace using nitrogen as the pressurizing medium. After sintering the nitrogen was still injected in the furnace as a shielding gas during cooling. The samples obtained above were divided into three groups, the first group was not annealed, the second group was annealed in oxygen, and the third group was annealed in nitrogen. Each group of samples was submitted to the following procedures: ultrasonic cleaning with de-ionized water, XRD (Rigaku D/Max-2200, Japan) analysis, SEM (Philips XL30ESEM-TMP, Netherlands) observation, coating with silver electrodes on the two surfaces, testing varistor properties, making TEM samples, STEM (FEI Tecnai G2 TF30 S-Twin, USA) analysis. The varistor properties were characterized by testing the main parameters α, E_B and J_L using the varis-tor DC parameter meter (Huigao HG3516, China). The parameters for the XRD analysis are as follows: radiation CuKα, acceleration voltage 20 kV, scanning interval 0.5 °·min^{-1} and step size 0.05 °·step^{-1}.

Table 1. Doping contents of samples.

Sample	Doping content (mol. %)		
	TiO_2	Ta_2O_5	$CaCO_3$
#1	99.80	0.10	0.10
#2	99.60	0.20	0.20
#3	99.50	0.25	0.25
#4	99.40	0.30	0.30

RESULTS

Experimental results

Table 2 shows the values of the nonlinear coefficient α, the breakdown voltage E_B and the leakage current J_L for different samples sintered at different temperatures. The sintering time of all samples was 2 h. As can be seen from Table 2, when the sintering temperature is 1200 °C, TiO_2–Ta_2O_5–$CaCO_3$ varistor ceramics have the relatively best varistor performance (α = 7.5, E_B = 24.0 V·mm^{-1}, J_L = = 12.3 μA·cm^{-2} for sample #2). Subsequently, the varistor properties of sample #2 with a sintering temperature of 1200 °C were investigated after annealing in oxygen and nitrogen for 2, 2.5, 3, 3.5, and 4 h, respectively.

Table 3 shows the electrical properties of the samples sintered at 1200 °C for 2 h and annealed in oxygen and nitrogen at 600, 700, 800, and 900 °C for 2, 2.5, 3, 3.5, and 4 h, respectively, where #2O2 and #2N2 represent annealing in oxygen for 2 h and in nitrogen for 2 h, respectively; #2O3 and #2N3 represent annealing in oxygen and nitrogen for 3 h, respectively, and similar for #2O2.5, #2N2.5, #2O3.5, #2N3.5, #2O4, and #2N4. As can be seen from Table 3, the samples annealed at the same temperature for the same time in oxygen and nitrogen show slight differences in the nonlinear coefficient α and the breakdown voltage E_B. The sample #2O3 annealed at 700 °C for 3 h in oxygen

Table 2. Electrical properties of samples with different sintering temperatures – E_B (V·mm^{-1}), J_L (μA·cm^{-2}).

Sample	1100 °C			1150 °C			1200 °C			1250 °C		
	α	E_B	J_L	α	E_B	J_L	α	E_B	J_L	α	E_B	J_L
#1	4.8	31.2	14.6	5.7	30.2	13.4	6.5	25.5	12.9	6.1	24.3	13.1
#2	5.0	29.2	14.5	5.6	30.6	13.8	7.5	24.0	12.3	6.3	24.1	12.8
#3	5.1	28.0	14.2	6.2	28.5	13.1	7.1	24.3	12.7	6.9	23.5	12.0
#4	4.9	29.4	14.6	6.4	29.8	12.9	6.7	23.8	12.2	7.1	22.4	12.5

Table 3. Electrical properties of samples annealed in oxygen and in nitrogen – E_B (V·mm^{-1}), J_L (μA·cm^{-2}).

Sample	Time	600 °C			700 °C			800 °C			900 °C		
		α	E_B	J_L	α	E_B	J_L	α	E_B	J_L	α	E_B	J_L
#2O2	2 h	8.5	23.2	10.2	8.8	23.5	9.8	8.6	22.3	11.5	8.0	24.3	11.8
#2N2	2 h	8.1	24.5	10.8	8.8	24.2	10.2	8.7	23.5	11.2	8.3	23.6	10.9
#2O2.5	2.5 h	9.0	24.4	9.8	9.6	23.7	9.5	8.8	22.7	11.1	8.5	24.5	10.6
#2N2.5	2.5 h	9.3	24.1	9.8	9.4	23.5	9.5	9.0	24.5	10.9	8.5	22.8	10.7
#2O3	3 h	9.9	25.2	9.1	11.2	22.6	8.7	10.2	22.5	9.5	9.6	22.3	10.5
#2N3	3 h	9.6	24.9	9.3	10.9	20.5	8.9	10.0	23.1	9.8	9.5	24.1	10.9
#2O3.5	3.5 h	9.6	23.7	9.5	10.5	21.9	9.2	9.8	21.5	10.2	9.0	21.6	11.3
#2N3.5	3.5 h	9.4	24.0	9.6	10.5	21.7	8.8	9.6	20.9	10.3	9.2	23.7	11.0
#2O4	4 h	9.1	24.3	9.8	10.1	22.5	9.4	9.4	23.0	10.5	9.1	22.9	11.4
#2N4	4 h	8.9	24.5	10.5	10.2	23.4	9.6	9.5	21.8	10.5	8.7	24.0	11.5

(denoted #2O73 in the sequel) has the best varistor performance with α = 11.2, E_B = 22.6 V·mm^{-1} and J_L = = 8.7 μA·cm^{-2}, which is superior to previous findings [24-26]. The sample #2N3 annealed at 700 °C for 3 h in nitrogen (denoted #2N73 in the sequel) has comparable performance with α = 10.9, E_B = 20.5 V·mm^{-1}, and J_L = = 8.9 μA·cm^{-2}. #2O73 and #2N73 are both superior to the unannealed sample #2. The result showed that annealing significantly improves the varistor performance of TiO_2–Ta_2O_5–$CaCO_3$ varistor ceramics. With the increase of the annealing temperature and the annealing time, the α value starts to decrease, which indicates that the annealing temperature and the annealing time have a significant influence on the varistor performance of the samples.

The average barrier height Φ_B of grain boundary of unannealed samples and samples annealed in oxygen and nitrogen is listed in Table 4. Φ_B was calculated via the formula

$$J = A^* T^2 \exp [(\beta E^{1.2} - \Phi_B / k T_K],$$

where A^* and k represent the Richardson constant and the Boltzmann constant, respectively, and T_K represents the absolute temperature. The two groups of electric current J and electric field E were tested at the same temperature. The values of β and Φ_B were calculated. Three Φ_B values were obtained and the average Φ_B was calculated for each sample.

Table 4. Effect of annealing on grain boundary barrier Φ_B (eV).

Sample	unannealed	600 °C	700 °C	800 °C	900 °C
#2	0.58	–	–	–	–
#2O3	–	0.89	1.49	1.41	1.37
#2N3	–	0.85	1.38	1.35	1.32

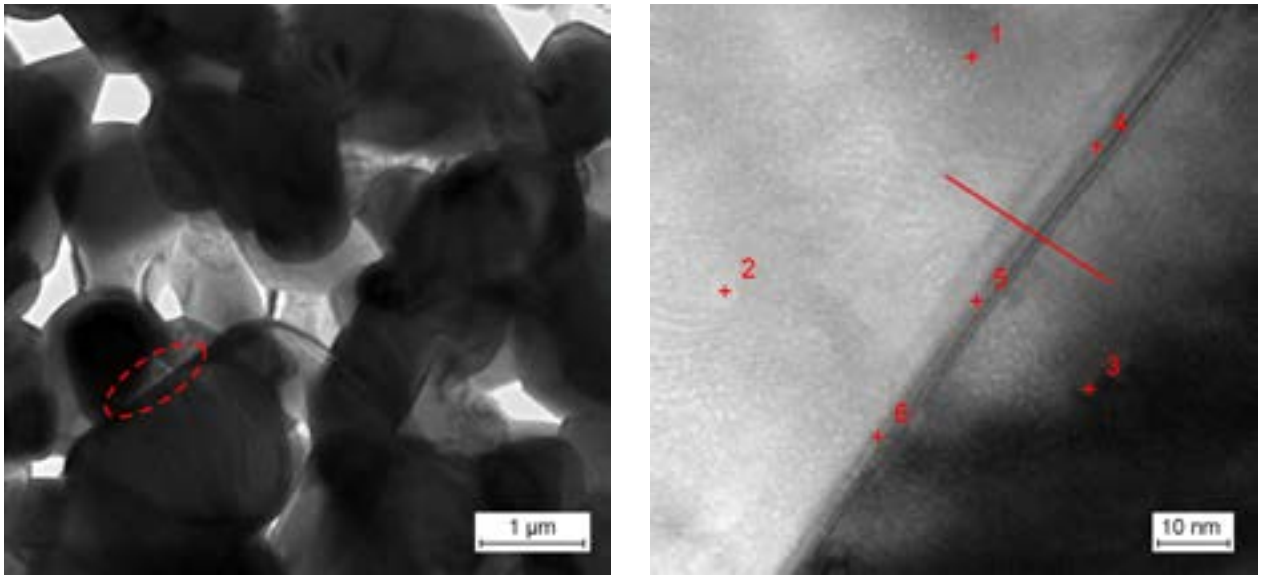

a)

Figure 1. STEM-EDS images of TiO_2–Ta_2O_5–$CaCO_3$ ceramics: a) unannealed (#2), annealed at 700 °C for 3 h in oxygen (b) (#2O73) and nitrogen (c) (#2N73). *(Continue on next page)*

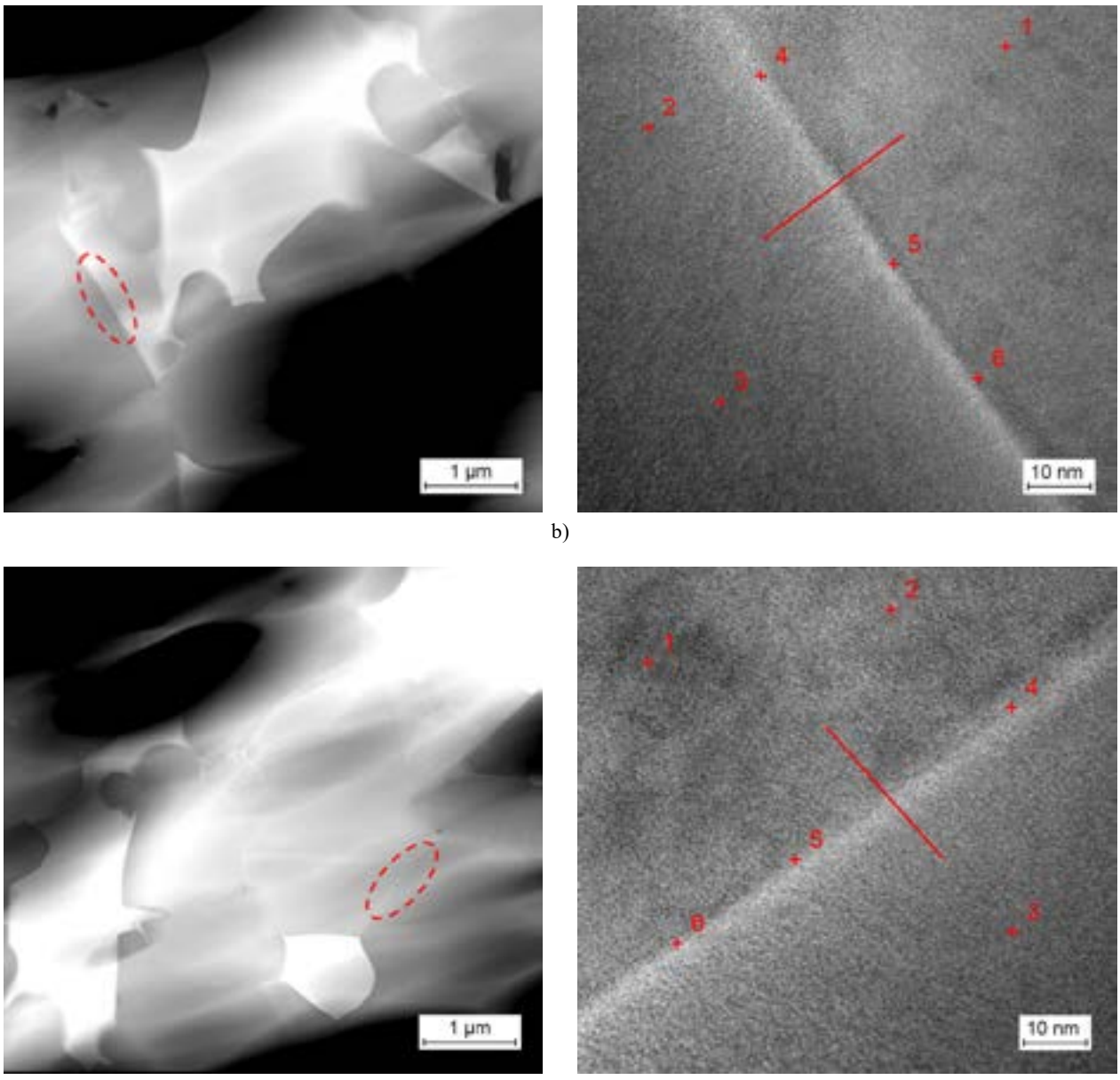

Figure 1. STEM-EDS images of TiO_2–Ta_2O_5–$CaCO_3$ ceramics: b) annealed at 700 °C for 3 h in oxygen (#2O73), c) nitrogen (#2N73).

STEM spot scanning analysis

Figure 1 is STEM-EDS (X-ray energy dispersive spectroscopy, in the sequel abbreviated as EDS) images of samples #2 (a), #2O73 (b) and #2N73 (c). The points 1, 2 and 3 are located inside the grains, while the points 4, 5 and 6 are located at grain boundaries in the figures. The element contents of each point are listed in Table 5. By analyzing element contents of the analyzed points, the contents of Ca at grain boundaries are found to be higher in the annealed samples #2O73 and #2N73 than in the unannealed sample #2. As expected, the O content of sample #2O73 is higher than that of sample #2 and #2N73 at the grain boundaries. Ca^{2+} ions are likely to be segregated at the grain boundary due to their large size. So the content of Ca^{2+} of the samples annealed in oxygen and nitrogen tends to decrease inside the grains, and tends to increase at the grain boundaries. Due to annealing in oxygen, the oxygen is of course enriched at the grain boundaries [27]. The nonlinear coefficient α of the annealed samples #2O73 and #2N73 is higher than that of the unannealed sample #2, which is mainly because the concentration of acceptor ions Ca^{2+} at the grain boundaries increases during annealing, thus increasing the acceptor density at the grain boundaries and the height of the grain boundary potential barrier. The α value of sample #2O73 is slightly higher than that of sample #2N73 due to oxygen enrichment at the grain boundaries that also increases the acceptor density and the height of grain boundary potential barrier during annealing.

Table 5. Element contents inside grains and at grain boundaries of sample unannealed (#2), annealed at 700 °C for 3 h in oxygen (#2O73) and annealed at 700 °C for 3 h in nitrogen (#2N73).

Position	Element (at. %)											
	OK			TiK			TaK			CaK		
	#2	#2O73	#2N73	#2	#2O73	#2N73	#2	#2O73	#2N73	#2	#2O73	#2N73
1	73.89	73.65	73.03	25.79	25.74	26.84	0.23	0.53	0.08	0.09	0.08	0.05
2	68.02	70.64	67.62	31.46	29.21	32.07	0.34	0.06	0.19	0.18	0.09	0.12
3	69.90	72.64	77.69	29.45	27.00	21.86	0.49	0.21	0.38	0.16	0.15	0.07
4	71.36	73.16	72.70	28.37	26.43	26.77	0.40	0.08	0.25	0.23	0.33	0. 28
5	69.58	70.80	68.55	30.09	28.36	30.95	0.07	0.43	0.12	0.26	0.41	0.38
6	70.96	71.04	67.18	28.39	28.51	32.18	0.35	0.17	0.39	0.30	0.28	0.25

STEM line scanning analysis

Figure 2 shows the line scan graphs of samples #2, #2O73 and #2N73 across the grain boundary. As can be seen from the figure, after annealing the content of Ca at the grain boundary is relatively higher; the oxygen content increases slightly at the grain boundary of sample #2O73 annealed in oxygen. The grain boundary width of sample #2O73 and #2N73 was estimated to be about 4.5 nm and 5.0 nm, based on the Ca content at the grain boundary.

XRD analysis

Figure 3 shows the XRD patterns of samples #2 (a), #2O73 (b) and #2N73 (c). It can be seen from Figure 3 that no diffraction peak of second phase is found after

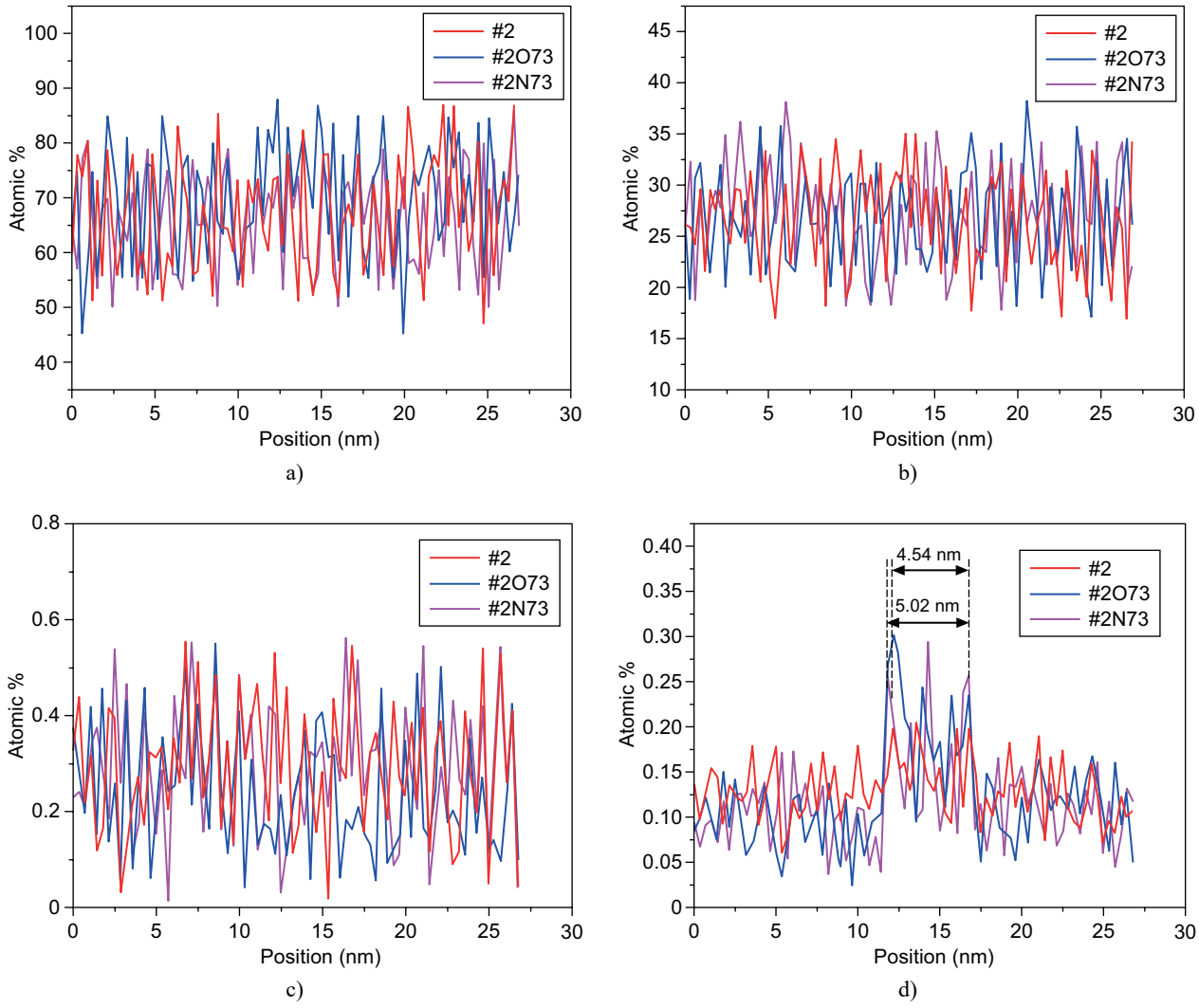

Figure 2. Line scan graphs of sample #2, #2O73 and #2N73 across grain boundaries.

annealing in oxygen or nitrogen. The diffraction peaks of sample #2O73 annealed in oxygen or #2N73 annealed in nitrogen are relatively smoother compared to those of the unannealed sample #2, and the strength of background peaks of #2O73 and #2N73 is significantly lower than that of #2. Table 6 shows the correlation parameters of the strongest diffraction peaks near 2θ = 27.5° for samples #2, #2O73 and #2N73. The diffraction peak intensity increases and the full width at half maximum (FWHM) decreases slightly in samples #2O73 and #2N73, indicating that the grains (crystallites) are well developed and essentially free of micro strain.

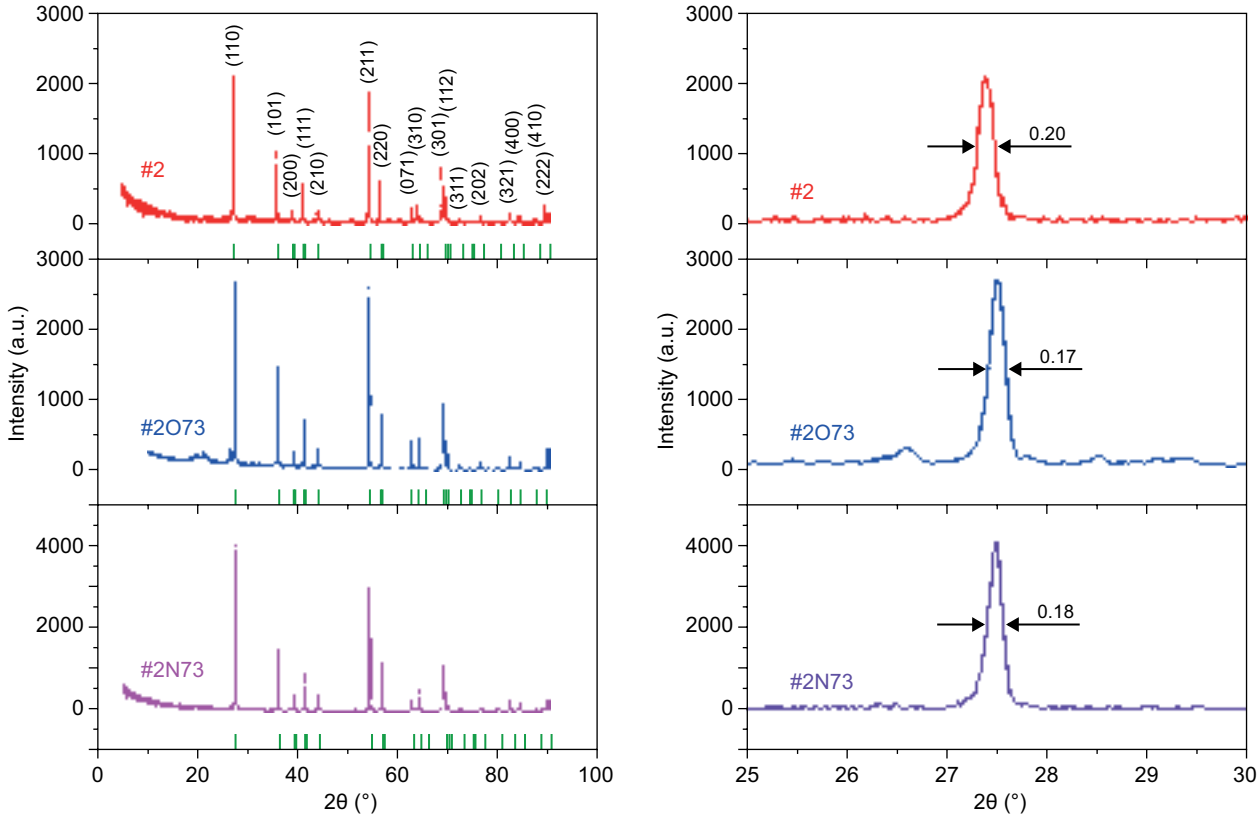

Figure 3. XRD patterns of TiO_2–Ta_2O_5–$CaCO_3$ ceramics unannealed (#2), annealed at 700 °C for 3 h in oxygen (#2O73) and nitrogen (#2N73).

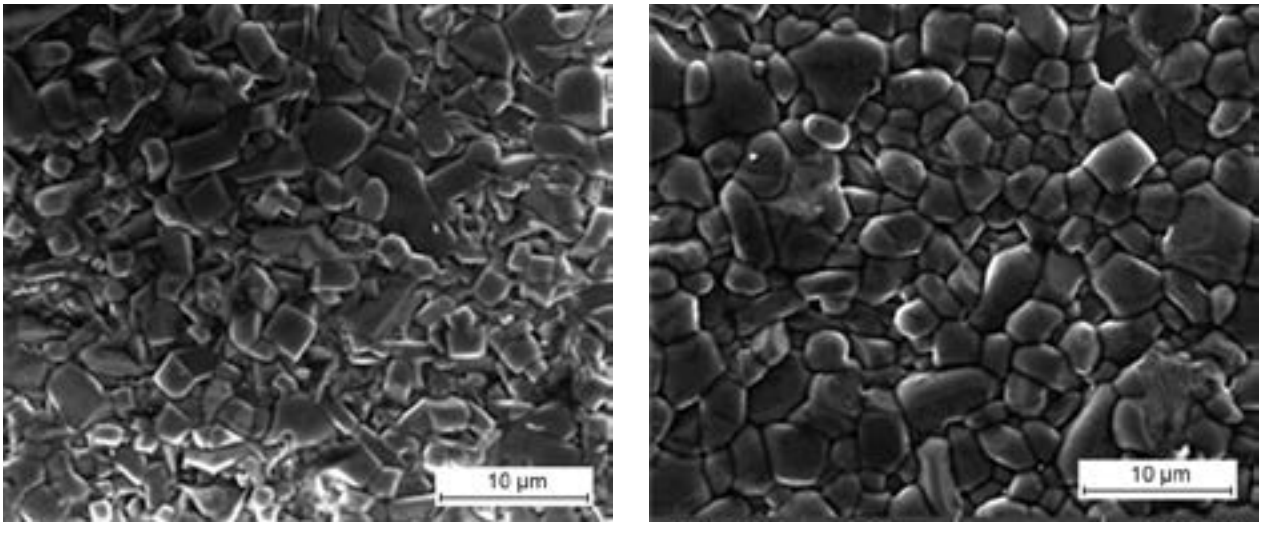

Figure 4. SEM images of TiO_2–Ta_2O_5–$CaCO_3$ ceramics: a) by HIP sintering and unannealed (#2), b) by HIP sintering and annealed at 700 °C for 3 h in oxygen (#2O73). *(Continue on next page)*

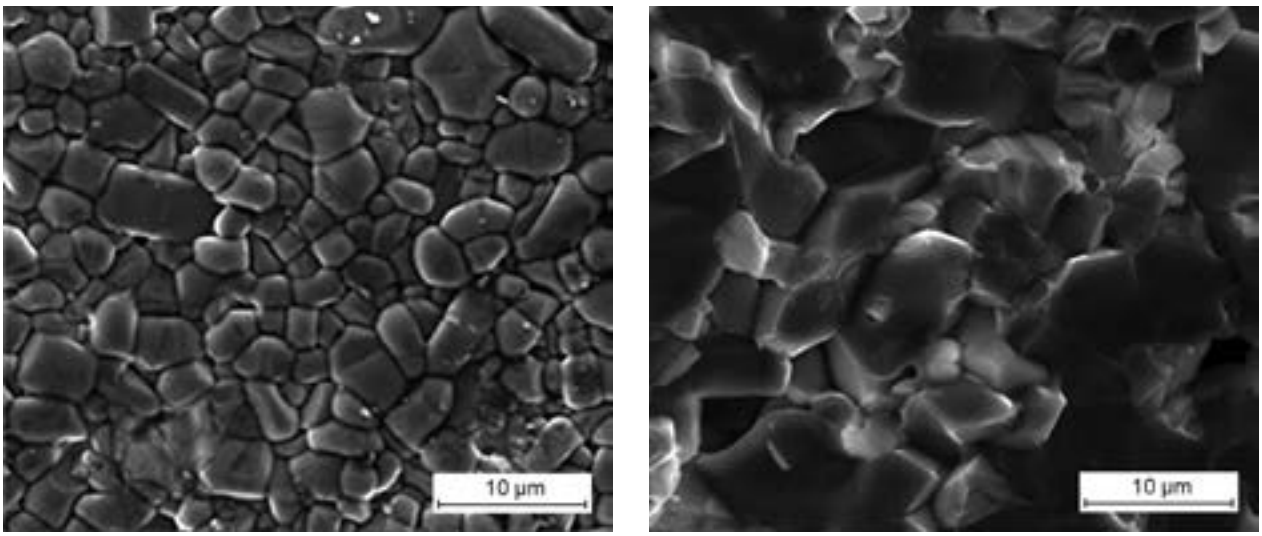

c) d)

Figure 4. SEM images of TiO_2–Ta_2O_5–$CaCO_3$ ceramics: c) by HIP sintering and annealed at 700°C for 3 h in nitrogen (#2N73), d) by pressureless sintering and unannealed.

Table 6. Diffraction peak change near 2θ = 27.5°of sample unannealed (#2), annealed at 700 °C for 3 h in oxygen (#2O73) and annealed at 700 °C for 3 h in nitrogen (#2N73).

Sample	2θ (°)	Peak height	FWHM (°)
#2	27.38	2124.51	0.20
#2O73	27.51	2743.66	0.17
#2N73	27.49	4012.96	0.18

SEM analysis

Figure 4 shows SEM micrographs of samples #2 (a), #2O73 (b), and #2N73 (c). From Figures 4a-c it is evident, that the grain structures of the three samples are relatively dense and the porosity is very low. Comparing (a), (b) and (c), it can be seen that the grains of samples #2O73 and #2N73 are bigger with a more uniform size than those of the unannealed sample #2, which is conducive to good electrical properties.

CONCLUSION

Hot isostatic pressing (HIP) and post-annealing can improve the microstructure of TiO_2–Ta_2O_5–$CaCO_3$ varistor ceramics. Using HIP TiO_2–Ta_2O_5–$CaCO_3$ varistor ceramics with uniform microstructure, fine grain and low porosity can be obtained. During annealing, the acceptor ions Ca^{2+} with larger radius are further segregated towards the grain boundaries, which increases the density of acceptor state and the height of the potential barrier at the grain boundaries. Therefore the nonlinear coefficient α increases. After annealing in the oxygen, the oxygen enrichment at the grain boundaries is also helpful to increase the grain boundary potential barrier, thus further increasing the α value. Increasing the grain boundary barrier reduces the background current, thus reducing the leakage current J_L. Annealing at a suitable temperature for a suitable time can make the grains grow appropriately and the grain size uniform, which results in a decrease of the number of grain boundaries and the total area of grain boundaries. Therefore the breakdown voltage E_B tends to decrease. As the doping content of Ta_2O_5 and $CaCO_3$ is 0.20 mol. %, respectively, and the sintering temperature is 1200 °C, TiO_2–Ta_2O_5–$CaCO_3$ varistor ceramics annealed at 700 °C for 3 h in oxygen possesses the best varistor performance, with α = 11.2, E_B = 22.6 V·mm^{-1} and J_L = 8.7 μA·cm^{-2}.

Acknowledgements

The present work was supported by the Agricultural Joint Programs of Yunnan Province [grant number 2018FG001-063], the University-Level Research Project [grant number 112004], the Applied Basic Research Programs of Yunnan Province [grant number 2019FB067], the Training Program of Young and Middle Aged Academic and Technological Leaders in Yunnan Province [grant number 2017HB030] and the High Level Innovative One-Ten-Thousand Youth Talents of Yunnan Province [grant number 2020].

REFERENCES

1. Gong Y.Y., Chu R.Q., Xu Z.J., Dou T.F., Zeng W.J., Zhang X.N., Hao J.G., Li G.R. (2016): Varistor, dielectric, and luminescent properties of Pr_6O_{11}-doped TiO_2 multifunctional ceramics. Journal of the American Ceramic Society, 99, 2995-3001. doi: 10.1111/jace.14251
2. Li Y.D., Zhu D.C., Xiang X., Wang J.S. (2016): Influence of Sm_2O_3 on electrical performance of (Nb, Si)-doped

TiO_2-based varistor. Journal of Materials Science: Materials in Electronics, 27, 3355-3360. doi: 10.1007/s10854-015-4165-y
3. Santana M.A.A., Dos Santos F.S.N., Sousa V.C., Chui Q.S.H. (2008): Variability sources of DC voltage-current measurements in the study of TiO_2-based varistors. Measurement, 41, 1105-1112. doi: 10.1016/j.measurement.2008.03.006
4. Yan M.F., Rhodes W.W. (1982): Preparation and properties of TiO_2 varistors. Applied Physics Letter, 40, 536-537. doi: 10.1063/1.93134
5. Bueno P.R., Varela J.A., Longo E. (2008): SnO_2, ZnO and related polycrystalline compound semiconductors: An overview and review on the voltage-dependent resistance (non-ohmic) feature. Journal of the European Ceramic Society, 28, 505-529. doi: 10.1016/j.jeurceramsoc.2007.06.011
6. Cassia-Santos M.R., Sousa V.C., Oliveira M.M., Sensato F.R., Bacelar W.K., Gomes J.W., Longo E., Leite E.R., Varela J.A. (2005): Recent research developments in SnO_2-based varistors. Materials Chemistry and Physics, 90, 1-9. doi: 10.1016/j.matchemphys.2003.12.014
7. Metz R., Koumeir D., Morel J., Pansiot J., Houabes M., Hassanzadeh M. (2008): Electrical barriers formation at the grain boundaries of co-doped SnO_2 varistor ceramics. Journal of the European Ceramic Society, 28, 829-835. doi: 10.1016/j.jeurceramsoc.2007.05.024
8. Yang S.L., Wu J.M. (1995): Effects of Nb_2O_5 in (Ba, Bi, Nb)-added TiO_2 ceramic varistors. Journal of Materials Research, 10, 345-352. doi: 10.1557/JMR.1995.0345
9. Meng F.M., Lu F., Xiao L., Sun Z.Q. (2009): Influence of soaking time on nonlinear electrical behavior and dielectric properties of TiO_2-based varistor ceramics. Journal of Central South University of Technology, 16, 0897-0901. doi: 10.1007/s11771−009−0149−5
10. Wang W.Y., Zhang D. F., Xu T., Li X.F., Zhou T., Chen X.L. (2002): Effect of temperature on nonlinear Electrical behavior and dielectric properties of (Ca,Ta)-doped TiO_2 ceramics. Materials Research Bulletin, 37, 1197-1206. doi: 10.1016/S0025-5408(02)00731-6
11. Navale S.C., Murugan A.V., Ravi V., (2007): Varistors based on Ta-doped TiO_2. Ceramics International, 33, 301-303. doi: 10.1016/j.ceramint.2005.07.026
12. Luo S.H., Tang Z.L., Li J.Y., Zhang Z.T. (2008): Effect of Ta_2O_5 in (Ca, Si, Ta)-doped TiO_2 ceramic varistors. Ceramics International, 34, 1345-1347. doi:10.1016/j.ceramint.2007.03.005
13. Zhao J.Z., Wang B.X., Lu K. (2014): Influence of Ta_2O_5 doping and microwave sintering on TiO_2-based varistor properties. Ceramics International, 40, 14229-14234. doi: 10.1016/j.ceramint.2014.06.012
14. Gong Y.Y., Chu R.Q., Xu Z.J., Sun J., Chao F.X., Ma S., Hao J., Li H.Y., Li G.R. (2015): Electrical properties of Ta_2O_5-doped TiO_2 varistor ceramics sintered at low-temperature. Ceramics International, 41, 9183–9187. doi: 10.1016/j.ceramint.2015.03.082
15. Gaikwad A.B., Navale S.C., Ravi V. (2005): TiO_2 ceramic varistor modified with tantalum and barium. Materials Science and Engineering B,123, 50-52. doi: 10.1016/j.mseb.2005.06.015
16. Luo S.H., Yao W.W., Li H.Y., Zhang Z.T., Xiong X.Z. (2005): The role of niobium in (Ca, Si, Ce, Nb)-doped TiO_2 varistors. Key Engineering Materials, 280-283, 297-300. doi: 10.4028/www.scientific.net/KEM.280-283.297
17. Wang W.Y., Zhang D.F., Xu T., Li X.F., Zhou T., Chen X.L. (2002): Nonlinear electrical behavior and dielectric properties of (Ca, Ta)-doped TiO_2 ceramics. Journal of Alloys and Compounds, 335, 210-215. doi: 10.1016/S0925-8388(01)01827-8
18. Zheng M.J., Zhang G.Z., Wang X., Wan J.X., Wu H., Liu C. (2017): Effects of post-deposition annealing on ZrO_2/n-GaN MOS capacitors with H_2O and O_3 as the oxidizers. Nanoscale Research. Letters.12, 267-271. doi: 10.1186/s11671-017-2024-x
19. Priyadarshini D.M., Ramanjaneyulu M., Ramachandra M.S.R, Nandita D.G. (2017): Effect of annealing ambient on SnO_2 thin film transistors. Applied Surface Science. 418, 414-417. doi: 10.1016/j.apsusc.2016.11.233
20. Hosokawa A., Takagi K., Kuriiwa T. (2017): Nanocomposite Nd-Fe-Ti-B magnets produced by melt spinning and flash annealing. Journal of Magnetism and Magnetic Materials, 439,220-227. doi: 10.1016/j.jmmm.2017.05.023
21. Mannam R., Kumar E.S., Nandita D.G., Ramachandra R.M.S. (2017): Reversible p-type conductivity in H passivated nitrogen and phosphorous codoped ZnO thin films using rapid thermal annealing. Applied Surface Science, 400, 312–317. doi: 10.1016/j.apsusc.2016.12.146
22. Li D., Dai S., Goullet A., Carette M., Granier A., Landesman J. P. (2018): Annealing and biasing effects on the structural and optical properties of PECVD-grown TiO_2 films from TTIP/O_2 plasma. Journal of Materials Science: Materials in Electronics, 29,13254-13264. doi: 10.1007/s10854-018-9449-6
23. Mohsen A., Mohammad A., Siti Nor Qurratu A. A.A., Chiam S. L., Ahmad Z.A., Pung S.Y. (2019): Influence of annealing temperature on morphological and photocatalytic activity of sputter-coated $CaCu_3Ti_4O_{12}$ thin film under ultraviolet light irradiation. Ceramics International, 45, 20697-20703. doi:10.1016/j.ceramint.2019.07.053
24. Zhao J.Z., Wang B.X., Lu K. (2014): Influence of Ta_2O_5 doping and microwave sintering on TiO_2-based varistor properties. Ceramics International, 40, 14229-14234. doi: 10.1016/j.jallcom.2014.06.102
25. Lan D.J., Wan S.Q. (2014): Investigation of low temperature sintering of low voltage varistor based on TiO_2. Advanced Materials Research, 852, 12-16. doi: 10.4028/www.scientific.net/amr.852.12
26. Kang K.Y., Yan J.K., Gan G.Y., Du J.H., Zhang J.M., Liu Y.C. (2016): Ge-added TiO_2–Ta_2O_5–$CaCO_3$ varistor ceramics. Ceramics International, 42,4739-4747. doi: 10.1016/j.ceramint.2015.11.151
27. Zhao J.Z., Zhang C.G., Hu C.Y., Lu K. (2017): Effect of thermal treatmenton TiO_2 varistor propertiesin different atmospheres. Journal of the European Ceramic Society, 37, 3353-3359. doi: 10.1016/j.jeurceramsoc.2017.04.021